Fabrication of Graphene Field Effect Transistors on Boron Nitride Substrates

Christopher Addiego
Physics, Carnegie Mellon University

NNIN REU Site: NanoTech User Facility, University of Washington, Seattle, WA
NNIN REU Principal Investigator: Prof. Xiaodong Xu, Physics, University of Washington
NNIN REU Mentor: Grant Aivazian, Physics, University of Washington
chris.addiego@comcast.net, xuxd@uw.edu, aivazian@uw.edu

Abstract:

Graphene is a two dimensional crystal of carbon atoms that has applications to new electronics and optoelectronics when fabricated as a field effect transistor (FET) [1]. The quality of these FETs is quantified partly by the carrier mobility of the device. The goal of this project is to determine a procedure for fabricating graphene FETs on hexagonal boron nitride (h-BN) substrates based on Dean et al. [2] in order to create devices with improved carrier mobility. A combination of chemical solvents and annealing procedures were used to clean the devices during fabrication. We found that only applying the chemical solvents yielded the devices with the highest carrier mobility (~ 500 cm^2/Vs). However, this value is much less than that of typical graphene FETs, indicating our procedure can still be improved.

Introduction:

Graphene is a monolayer of graphite composed of a single layer of carbon atoms arranged in a honeycomb lattice. Graphene has many remarkable mechanical, electronic, and optoelectronic properties stemming from its structure including its high carrier mobility and optical transparency in the visible to infrared wavelength range [1]. These properties make it an attractive material for use in high frequency electronics and devices requiring transparent conductive films [1].

A general measure for the quality of graphene FETs fabricated in the lab is the carrier mobility of the device. Despite graphene's high intrinsic carrier mobility, the carrier mobility of the devices fabricated on silicon dioxide (SiO_2) substrates is limited by scattering caused by the surface roughness, charged impurities, and interactions with phonons of the SiO_2 substrate [2]. Residues deposited during the fabrication process also limit carrier mobility [3]. Our goal was to improve the carrier mobility of our grapheme FETs by fabricating them on h-BN substrates. Previous work by Dean et al. indicates that h-BN can act as a much better substrate for graphene devices than SiO_2 because it has comparable dielectric properties to SiO_2 while also having a smoother surface which should reduce carrier scattering within graphene.

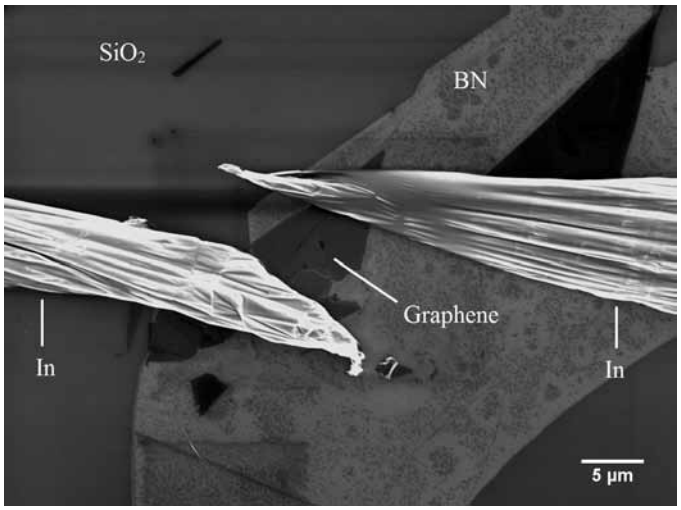

Figure 1: SEM of a graphene device on an h-BN substrate.

Device Fabrication:

Standard graphene FETs are fabricated by first exfoliating graphene onto 300 nm of SiO_2 on a doped silicon wafer, which acts as a back gate, and then writing gold electrical contacts with electron beam lithography (EBL) onto the graphene. The fabrication process we used for our h-BN devices was slightly more complex; graphene was first exfoliated onto a polymer stack and BN flakes were exfoliated onto 300 nm of SiO_2 on doped silicon. Graphene was identified first based on contrast and then later confirmed with Raman spectroscopy. The h-BN flakes were selected using an atomic force microscope (AFM) to have a thickness of 10-30 nm and minimal changes in thickness over the surface. Using the procedure outlined by Dean et al. [2], the graphene was transferred onto the h-BN flake and the polymer stack was dissolved. We decided not to use EBL to write our contacts because it would deposit additional residue onto the device. Instead, we used a micromanipulator to write indium contacts onto the device. A scanning electron microscope (SEM) image of a device can be seen in Figure 1.

To remove residues deposited during the fabrication procedure, we used a combination of chemical solvents and annealing in argon gas (Ar) and molecular hydrogen gas (H_2). Acetone (ACE) and isopropanol (IPA) were the primary solvents, and distilled water as used on select occasions. Annealing was done in a one-inch tube furnace at 350°C for 120 minutes. An AFM was used to identify the residues deposited during the fabrication process.

Results:

Once the devices had been fabricated, the conductance (G) of each device was measured, using a sensitive preamplifier, by maintaining a constant source-drain voltage while sweeping the gate voltage. The carrier mobility (μ) was calculated according to the formula shown in Figure 2 [3]. In the formula, $C = 115 \times 10^{-10}$ F/cm^2, L is the length of the device parallel to the current path, W is the width of the device perpendicular to the current path, and the derivative of G with respect to gate voltage is taken to be the slope of the highlighted region in Figure 3. In searching for the optimal fabrication procedure, we fabricated devices using different permutations on the basic fabrication procedure, altering the anneal parameters and the order in which we performed the annealing and graphene transfer.

$$\mu = \frac{1}{C}\frac{L}{W}\frac{\partial G}{\partial V_{gate}}$$

Figure 2: Equation defining carrier mobility.

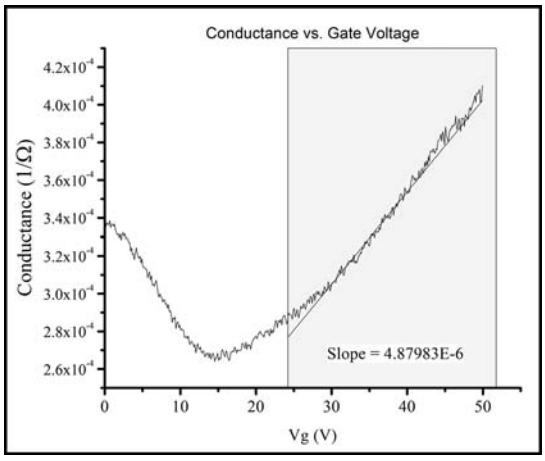

Figure 3: Example of conductance data from a device.

Conclusions:

As shown in Figure 3, we found that washing the h-BN flake in ACE and IPA prior to performing the transfer and then soaking in distilled water and rinsing with ACE and IPA after the graphene transfer and dissolving the polymer stack yields the highest carrier mobility (~ 500 cm^2/Vs). Although other variations of the procedure were tried, the processes described in Figure 4 were the only ones that produced useable devices. In addition, the highest carrier mobility attained by the devices fabricated using our procedure was significantly smaller than that of devices fabricated using the standard process. This suggests that further research is required to develop our fabrication procedure.

Acknowledgements:

I would like to thank Prof. Xu and Grant Aivazian, along with the other members of the Xu Lab and Mack Carter, for their guidance this summer. This project was funded by the National Nanotechnology Infrastructure Network Research Experience for Undergraduates (NNIN REU) Program and the National Science Foundation.

References:

[1] F. Bonaccorso, Z. Sun, T. Hasan, and A. C. Ferrari; "Graphene photonics and optoelectronics." Nature Photonics 4 (2010).

[2] C. R. Dean, et al. "Boron nitride substrates for high-quality graphene electronics." Nature Nanotechnology 5 (2010).

[3] K. I. Bolotin, et al. "Ultrahigh electron mobility in suspended graphene." Solid State Communications 146, pp 351-355, (2008).

Cleaning Processes Before Graphene Transfer	Cleaning Processes After Graphene Transfer and Polymer Dissolution	Carrier Mobility (cm^2/Vs)
Soak/rinse in ACE and IPA	Soak in distilled water, rinse in ACE and IPA	497.4
Soak/rinse in ACE and IPA	Anneal in Ar /H_2	322.2

Figure 4: A summary of the fabrication procedures that yielded useable devices.

PROC

TiO2-Based Core/Shell Nanowires for Adding Gas Sensing Capabilities to Silicon CMOS Circuitry

Satoshi Anada
Materials and Manufacturing Science, Osaka University, Osaka Prefecture, Japan

NNIN iREG Site: Penn State Nanofabrication Laboratory, The Pennsylvania State University (PSU), University Park, PA
NNIN iREG Principal Investigator: Theresa S. Mayer, Electrical Engineering and Materials Science and Engineering, PSU
NNIN iREG Mentor: Xiahua Zhong, Electrical Engineering, The Pennsylvania State University
Contact: anada@uhvem.osaka-u.ac.jp, tsm2@psu.edu, xxz138@psu.edu

Abstract:

Silicon/titanium dioxide (Si/TiO_2) core/shell nanowires were prepared by atomic layer deposition (ALD) of a TiO_2 shell on the surface of high-aspect-ratio Si nanowires that were obtained by deep reactive ion etching (DRIE) of a high resistivity Si substrate patterned using colloidal lithography. The microstructure of the TiO_2 was determined by transmission electron microscopy (TEM) technique. In the as-deposited sample, the shell of the nanowire was found to be amorphous TiO_2. After annealing in O_2 gas at 873 K for two hours, the amorphous phase transformed into a crystalline phase, identified as anatase TiO_2. As a result, it was found that the amorphous shell transformed into anatase TiO_2 by the annealing.

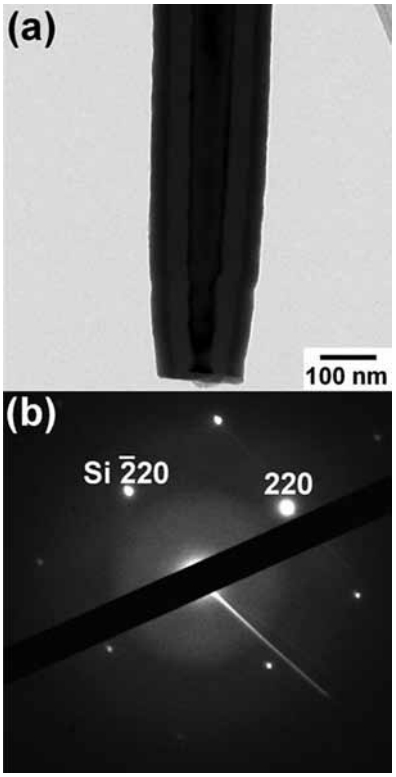

Figure 1: TEM observation of the nanowire before annealing.

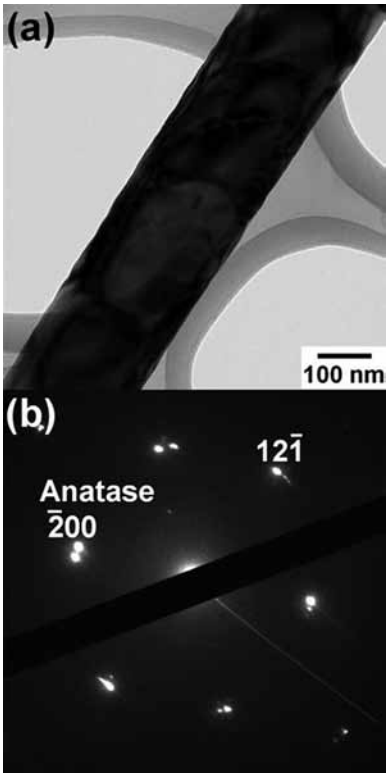

Figure 2: TEM observation of the nanowire after annealing at 873 K.

Introduction:

Electronic devices such as microprocessors, microcontrollers, static random-access memories, and other digital logic circuits are based on the complementary metal oxide semiconductor (CMOS) technology because of its low static power consumption and noise immunity. New functionalities obtained by integrating unconventional materials and devices with the Si circuitry will dramatically expand its capabilities and performance. For example, metal oxide materials designed to produce a large electronic response to chemical vapors offer sensing capabilities. However, the high temperatures required to fabricate high-sensitivity metal oxide nanowire sensors would damage the CMOS circuitry, which has made it difficult to effectively couple them in a single integrated circuit (IC) platform. Bottom-up synthesis of nanowires, composed of a diverse range of elemental or compound materials, offers a promising way to add sensing functions CMOS circuits. We have focused on using electric-field directed self-assembly to position arrays of individual nanowires synthesized using bottom-up methods at predefined locations on a CMOS substrate [1, 2].

In this project, Si nanowires coated by TiO_2 (Si/TiO_2 core/shell) were fabricated for gas sensor arrays on Si CMOS. The gas sensor performance of the wires is strongly dependent on the TiO_2 microstructural properties, including uniformity, thickness, composition, and atomic configuration [3]. The goal of this project was to clarify the relationship between the gas sensitivity and the TiO_2 microstructure. In the present study, the microstructure of different types of TiO_2-coated Si nanowires was investigated by TEM to understand the effect of thermal annealing on TiO_2 microstructure.

PROC

Experimental Procedure:

The nanowires were prepared by ALD of a TiO_2 shell on the surface of high-aspect-ratio Si nanowires that were obtained by deep reactive ion etching (DRIE) of a high resistivity Si substrate patterned using colloidal lithography. Thermal annealing was carried out at 873 K in O_2 gas for 7.2×10^3 s with a heating rate of 8.3×10^{-3} K s^{-1}. Then the substrate was allowed to cool to room temperature. The nanowires before and after the annealing were observed by TEM, capturing bright-field (BF) images and selected area diffraction (SAD) patterns.

Results:

Figure 1 shows the microstructure of the nanowire before annealing. In the BF image (a), it was found that the core of nanowire was surrounded by two shells whose contrasts are featureless. The length of the nanowire, diameter of the core and thickness of the inner and outer shells were about 5 μm, 80 nm, 40 nm and 30 nm, respectively. In the SAD pattern (b), a spot pattern and diffuse scattering disk pattern were detected. This spot pattern corresponds to that of crystalline Si <001>. The disk pattern can be attributed to the overlapping halo rings and background of the transmitted wave. These results indicate that the core was single-crystal Si and the shells were amorphous phases of the constituent materials. Further investigation is necessary to identify the exact composition of the amorphous shells; however, based on the nanowire fabrication process, the inner and outer amorphous shells are expected to be SiO_2 and TiO_2, respectively.

Figure 2 shows the microstructure of the nanowire after annealing at 873 K in O_2 gas. In the BF image (a), some grain-boundary and bend-contour contrast were observed, indicating the outer shell consists of coarse crystalline grains. All diffraction spots in the SAD pattern (b) could be indexed by anatase TiO_2 <012> diffraction spots. As a result, it was found that the outer amorphous shell transformed into coarse grains of anatase TiO_2 by annealing at 873 K. It should be noted that no significant changes in the core and the inner shell were detected following thermal annealing.

Conclusions and Future Work:

In this project, Si/TiO_2 core/shell nanowires were fabricated for gas sensor arrays. The nanowires were investigated by TEM focusing on the effect of annealing on the TiO_2 microstructure. As a result, the following conclusions were obtained:

(1) The fabricated nanowires before annealing consisted of three parts, namely, single-crystal silicon core, inner and outer amorphous shells.

(2) The outer amorphous shell transformed into coarse grains of anatase TiO_2 by annealing at 873 K.

In the future, these fabricated nanowires will be integrated onto lithographically patterned Si substrates using electric-field directed self-assembly and their gas sensitivity will be measured to clarify influence of TiO_2 microstructure.

Acknowledgements:

This work was supported by the National Nanotechnology Infrastructure Network International Research Experience for Graduates (NNIN iREG) Program, together with Nanotechnology Platform, Japan. I would like to thank Prof. Mayer, her research group, Kathleen Gehoski, Ke Wang, Nanofabrication Lab Staff, and the Material Research Institute.

References:

[1] T.J. Morrow, M. Li, J. Kim, T.S. Mayer, and C.D. Keating, "Programmed Assembly of DNA-coated Nanowire Devices," Science, 323, 352 (2009).

[2] M. Li, R.B. Bhiladvala, T. Morrow, J. Sioss, K.-K. Lew, J.M. Redwing, C.D. Keating, and T.S. Mayer, "Bottom-up Assembly of Large-area Nanowire Resonator Arrays," Nature Nanotechnology, 3, 88 (2008).

[3] G.F. Fine, L.M. Cavanagh, A. Afonja, and Russell Binions, "Metal Oxide Semi-Conductor Gas Sensors in Environmental Monitoring," Sensors, 10, 5469 (2010).

One-Step Synthesis of Nanostructured Graphene Nanocomposites for CO_2 Capture and Photoreduction

Hannah Bailey
Engineering Physics, Rose-Hulman Institute of Technology

NNIN REU Site: Nano Research Facility, Washington University in St. Louis, St. Louis, MO
NNIN REU Principal Investigator: Dr. Pratim Biswas, Energy, Environmental and Chemical Engr., Washington University in St. Louis
NNIN REU Mentor: Dr. Wei-Ning Wang, Energy, Environmental and Chemical Engineering, Washington University in St. Louis
Contact: baileyh@rose-hulman.edu, pbiswas@wustl.edu, wangwn@seas.wustl.edu

Introduction:

As knowledge of the effect that carbon emissions have on the ecosystem increases, greater attention is being drawn to decreasing carbon dioxide (CO_2) production [1]. Carbon capture and sequestration (CCS) is one method of reducing carbon emissions, often realized with amine adsorption [2], and followed by CO_2 underground storage [1]. CCS is energy intensive and has unknown associated risks [1]. An alternative process, carbon capture and conversion (CCC), can improve CCS using solar energy to reduce CO_2 to useable products, eliminating CO_2 storage risks while meeting energy needs with an available source [1]. CCC can be realized using semiconductor photocatalysis to absorb solar energy and produce electron-hole pairs supporting reduction and oxidation mechanisms [1].

We sought to improve the CCC catalyst by synthesizing a ternary-structured nanoball consisting of ethylenediamine functionalized reduced graphene oxide-titanium dioxide (EDA/rGO-TiO_2) using a one-step furnace aerosol reactor (FuAR) method. TiO_2 was used to provide a suitable semiconductor [1]; rGO provided a conductive support with high surface area and morphology to increase charge transfer and reduce agglomeration [3]; EDA functionalization provided surface groups to increase CO_2 adsorption [2]; FuAR synthesis allowed for fast, relatively inexpensive production that supports bulk implementation [3]. EDA/rGO-TiO_2 was tested as a CCC photocatalyst to determine its effectiveness.

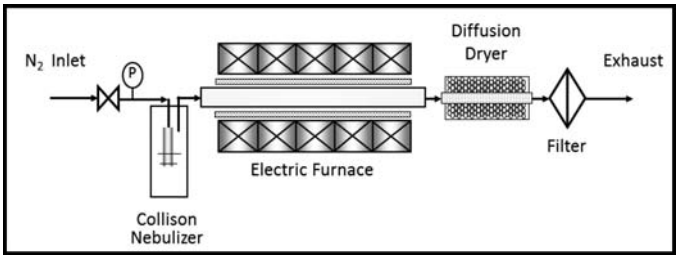

Figure 1: Furnace aerosol reactor.

Experimental:

EDA/rGO-TiO_2 was synthesized employing the FuAR system shown in Figure 1. We prepared a precursor solution by mixing 37.6 μL TiO_2 suspension (40 wt%), 10 mL EDA solution (≥ 99.5%), 50 mL GO suspension (1.4 wt%), and 140 mL deionized water in a covered beaker stirring magnetically at 4000 rpm for 24 hours. The solution was loaded into a Collison Nebulizer and the furnace was set to 200°C. Compressed nitrogen gas entered through a valve at a pressure of 14 psi, traveled into the Collison Nebulizer and atomized the solution into micrometer-sized droplets. The droplets flowed through the furnace wherein the droplet water evaporated, particles formed and passed through a diffusion dryer absorbing excess water before collection on a filter.

We repeated the procedure varying the furnace synthesis temperature to 150, 300, 400, 500, 600 and 800°C, and at 200°C furnace synthesis temperature varying the volumetric ratio of EDA to GO in solution from 10/50 to 15/50, 20/50, 25/50 and 30/50 EDA/GO. The rGO and rGO-TiO_2 particles were synthesized similarly at furnace temperatures of 200°C, 400°C and 600°C from solutions of 50 mL GO (1.4 wt%) and 150 mL deionized water, the latter incorporating 37.6 μL TiO_2 (40 wt%). TiO_2 particles were obtained by drop-casting 10 mg TiO_2 onto a filter. EDA/rGO-TiO_2 was characterized using scanning electron microscopy (SEM), transmission electron microscopy (TEM), Fourier transform infrared (FTIR) spectroscopy and Raman spectroscopy.

We tested EDA/rGO-TiO_2 as a catalyst in CO_2 photoreduction employing the reactor depicted in Figure 2. EDA/rGO-TiO_2 was placed on deionized water-dampened glass wool inside the reaction chamber. Compressed CO_2 was set to maximum flow (> 42 mL/min) into a water bubbler using a mass flow controller to generate a mixture and flow into the chamber to purge the system. After one hour, the ultraviolet lamp was turned on illuminating EDA/rGO-TiO_2. The CO_2 flow rate was lowered to 3 mL/min. The reaction duration was 12 hours during which gas concentrations were recorded after passing through the chamber using gas chromatography (GC).

Results and Discussion:

TEM, given in Figure 3, and SEM showed the GO sheets crumpled into nanoballs without agglomeration and dispersed with TiO_2, which indicates EDA/rGO-TiO_2 maintained high surface area for CO_2 adsorption, amine functionalization and charge transfer with TiO_2 intercalation. FTIR and Raman spectra in Figure 4 allowed for surface functional group characterization of EDA/rGO-TiO_2. EDA/rGO-TiO_2 FTIR and Raman spectra contained characteristic TiO_2 peaks indicating successful TiO_2 incorporation. EDA/rGO-TiO_2 FTIR spectra displayed a C = C graphene peak indicating that GO was reduced; characteristic C-N, N-H and CH_2 peaks evidenced successful EDA functionalization. EDA/rGO-TiO_2 Raman spectra showed characteristic D and G bands of rGO. The greater D/G band intensity ratio indicates a greater number of surface functional groups and defects in the nanoballs and provided evidence of EDA incorporation and remaining GO oxide groups. Spectral analysis of varying parameters showed that synthesis temperature and solution composition effected particle composition. EDA and reduction evidence became more intense and showed consistency at temperatures greater than 200°C and as the EDA/GO ratio increased, which indicated better EDA functionalization and GO reduction with greater temperature and EDA concentration.

Spectra comparison over periods of time showed EDA/rGO-TiO_2 maintained similar surface functional groups over 10 days and exhibited numerous variations after 40 days. This indicated EDA/rGO-TiO_2 has relatively stable surface composition over short periods of time, but significantly alters over extended periods of time. GC measurements using EDA/rGO-TiO_2 synthesized at 200°C with a 10/50 EDA/GO ratio showed carbon monoxide production indicating that the particles are functional catalysts for CO_2 reduction. Repeating the experiment with the same particles showed positive CO_2 reduction results indicating that the particles can be regenerated for reuse.

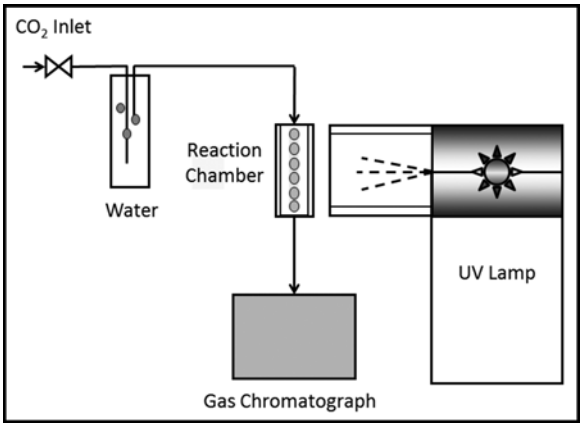

Figure 2: CO_2 photoreduction reactor.

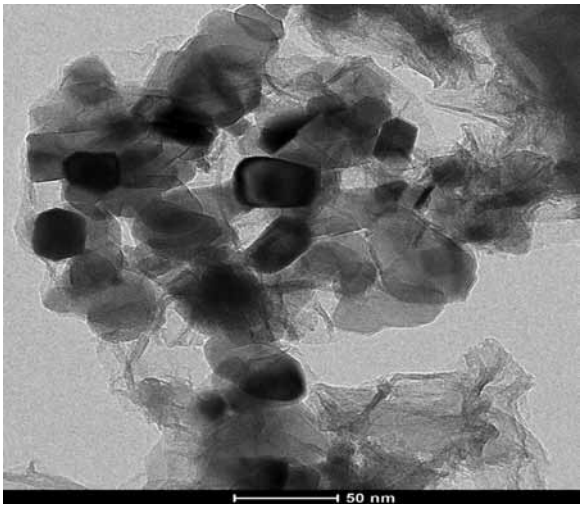

Figure 3: TEM image of EDA/rGO-TiO_2.

Acknowledgments:

I would like to thank Dr. Wei-Ning Wang, Dr. Pratim Biswas and Amruta Joshi from the Aerosol and Air Quality Research Lab for their guidance and expertise. I would also like to thank Dee Stewart, Nathan Reed, Kate Nelson, Howard Wynder and Sanmathi Chavalmane from the Nano Research Facility, the National Nanotechnology Infrastructure Network Research Experience for Undergraduates (NNIN REU) Program and National Science Foundation.

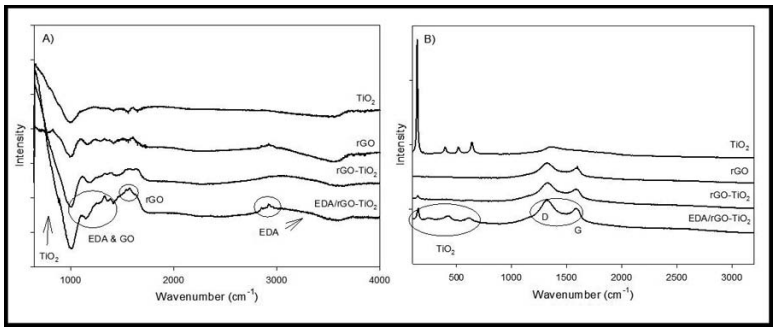

Figure 4: a) FTIR and b) Raman spectra varying particle composition.

References:

[1] W.-N. Wang, J. Park, and P. Biswas, "Rapid Synthesis of Nanostructured Cu-TiO_2-SiO_2 Composites for CO_2 Photoreduction by Evaporation Driven Self-assembly," Catalysis Science and Technology, 1 (4): 593-600 (2011).

[2] Y. Zhao, H. Ding, Q. Zhong, "Preparation and characterization of aminated graphite oxide for CO_2 capture," App.Surface Sci., 258 (10): 4301-4307 (2012).

[3] W.-N.Wang, Y. Jiang, and P. Biswas, "Evaporation-Induced Crumpling of Graphene Oxide Nanosheets in Aerosolized Droplets: Confinement Force Relationship," Journal of Physical Chemistry Letters, 3 (21): 3228-3233 (2012).

MOSFET: Fabrication Process and Performance Analysis

Kristofer Chow
Electrical Engineering, American River College

NNIN REU Site: UCSB Nanofabrication Facility, University of California, Santa Barbara, CA
NNIN REU Principal Investigator: Prof. Mark Rodwell, Electrical and Computer Engineering, University of California, Santa Barbara
NNIN REU Mentor: Dr. Doron Cohen-Elias, Electrical and Computer Engineering, University of California, Santa Barbara
Contact: krischow3@gmail.com, rodwell@ece.ucsb.edu, doroncohenelias@ece.ucsb.edu

Abstract:

The focus of this project was to determine the optimal gate region wet etch time, using the trench method, for the metal-oxide semiconductor field-effect transistor (MOSFET) fabrication process. The gate region, or trench, etching was time-dependent because too little time resulted in short-circuiting devices, while too much time resulted in lower-performing devices. The semiconductor parameter analyzer (SPA) examined the transistors' efficiency by generating current-voltage (I-V) graphs. No devices were successfully produced, but the optimal etching time range was found to exist between 15 and 25 seconds for this project's sample composition.

Introduction:

Scaled MOSFETs enable electronics to be made smaller and consume less power. Nanotechnology researchers solve problems that arise during the attempt to scale down the transistors, decreasing transistors' threshold voltages V_{TH}. With lower V_{TH}, devices have the capability to consume lower amounts of power, resulting in greater device efficiency. The most significant problem associated with this project was the etch stop thickness. Effective etch stops are at least 5 nm thick, preventing etchants from penetrating through the surface. Since the samples' layer was 2 nm thick, the mordant etched through the indium gallium arsenide (InGaAs) and the indium phosphide (InP) of the gate region. Caution was taken to ensure that the etching removed the etch stop, without penetrating into the channel region. By alternating the trench etch time with multiple samples, an optimal gate region etch time was attempted to be found and employed for future processes.

Experimental Procedure:

The trench method consisted of four photolithography stages: isolation, gate region definition, gate metal deposition, and source/drain metal deposition. During each photolithography step, masks containing prints for a set of devices were used to expose the same print multiple times on the samples. Each print was designed for approximately 100 devices, and the total transistor count for each sample varied depending on the wafer size. The isolation process involved dry etching into the hard mask and wet etching the sample, using substance ratios of one part phosphoric acid (H_3PO_4): one part hydrogen peroxide (H_2O_2): 25 parts water (H_2O), until the etch level was in the barrier. This defined the active area of each device and varied the channel widths (5-25 μm). The gate region definition stage consisted of dry etching into the hard mask, and wet etching, using the same mordant from isolation, into the contact and etch stop layers of the exposed devices. This etching phase determined the channel lengths (0.3-1.0 μm); the etching was controlled by time, due to the thin etch stop layer.

The third photolithography step occurred after the hard mask removal, approximately 4 nm hafnium oxide (HfO_2) deposition, and 15 minute annealing at 400°C with forming gas purging. Following the oxide annealing, gate metal — nickel (Ni) — was deposited above the trench region, including the sides along the device for functioning and measurement purposes. The excess Ni was lifted-off and the last photolithography step protected areas where the source/drain metals were not supposed to cover. Hydrofluoric acid (HF) was used to remove some oxide in order to establish contact sites for the source/drain metals.

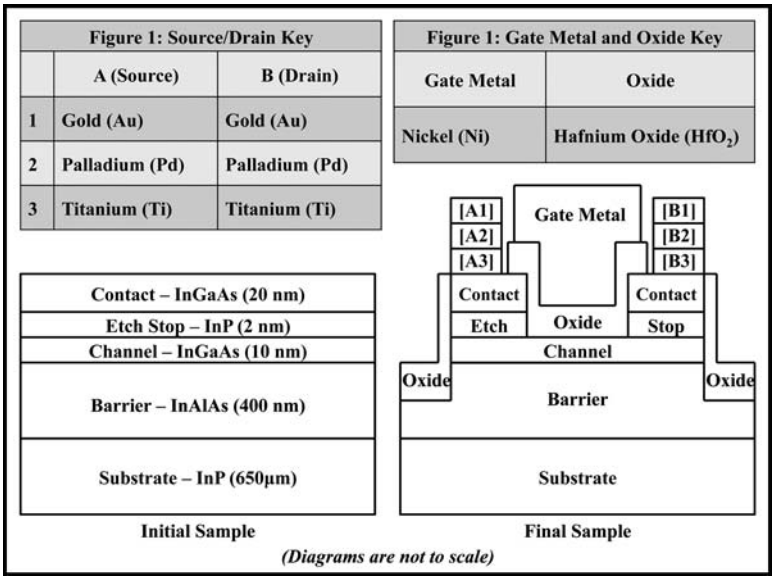

Figure 1: Initial and final stages of the MOSFET fabrication process.

Etch Time and Deposition Summary					
	Gate Region Etch Time	Oxide Deposition	Gate Metal Deposition	Source/Drain Metal Deposition	Measured by SPA?
Sample 1	10 seconds	3.5 nm HfO_2	64 nm Ni	25 nm Ti/ 30 nm Pd/ 50 nm Au	Yes
Sample 2	15 seconds	3.5 nm HfO_2	64 nm Ni	25 nm Ti/ 30 nm Pd/ 50 nm Au	Yes
Sample 3	25 seconds	3.5 nm HfO_2	75 nm Ni	N/A	No
Sample 4	25 seconds	4.5 nm HfO_2	95 nm Ni/ 75 nm Au	N/A	No

Figure 2: Summary of the samples' etching times and deposition thicknesses.

The source/drain metals — titanium (Ti), palladium (Pd), and gold (Au) — were deposited onto the sample, and the final lift-off removed the excess metal. Ti was deposited for its n^+ contact properties, Pd for its ability to prevent gold diffusion into the semiconductor [1], and Au for its non-oxidizing properties (Figure 2).

Results:

A total of four samples were fabricated during this research project. The first process consisted of two samples that experienced gate region etch times of 10 and 15 seconds. These wafers were tested with no gate voltage and their I-V graphs suggested resistor-like behaviors (see Figure 3). These results led to another process, consisting of a sample with 25 seconds of trench etching. Following gate metal deposition, the sample was examined under the scanning electron microscope (SEM): the gate metal along the sides of the devices did not connect to the Ni above the channel (see Figure 4); voltage could not be applied to the gate without potentially damaging the metal. The last sample also underwent 25 seconds of trench etching, but the gate metal and source/drain photoresist was lifted off during the oxide etching with HF. This unexpected result may have been due to poor photoresist development.

Conclusions:

Although no working transistors were produced, the experimental results obtained will help future researchers. The optimal gate region wet etch time was found to exist between 15 and 25 seconds after attempting to fabricate four samples. The maximum time was observed because the 15-second sample underwent another procedure: the HfO_2 was removed and the devices were wet etched for 10 additional seconds. No current was conducted through the devices when no gate voltage was applied.

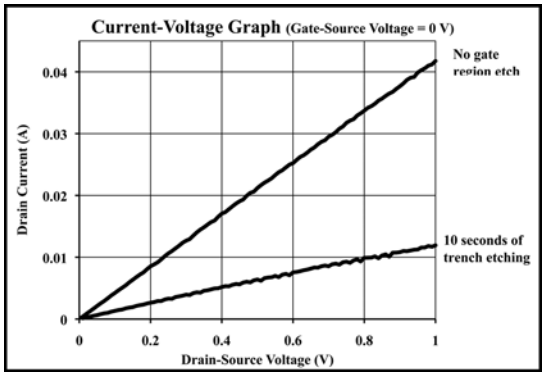

Figure 3: Performance comparison between a trenchless device and a 10-second etched device.

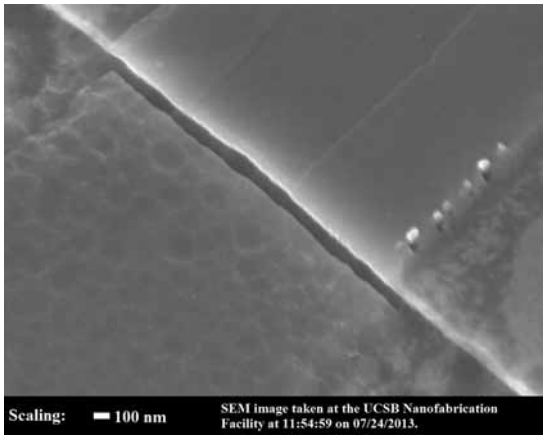

Figure 4: SEM of the third sample's gate metal discontinuity.

Scientific investigators can continue to construct MOSFETs, knowing they can achieve functioning devices with 25 seconds of etching, or they can alter the etch time parameter to define the most optimal trench etch time. Despite the knowledge this research provides, these results do not guarantee perfect-working devices; rather, this information improves the chances of fabricating more efficient MOSFETs.

Acknowledgements:

This project would not have been possible without the generous support from the National Nanotechnology Infrastructure Network Research for Undergraduates (NNIN REU) Program and the National Science Foundation (NSF). Professor Mark Rodwell and Dr. Doron Cohen-Elias deserve significant credit, as principal investigator and mentor, for their guidance and assistance throughout the course of this project. Melanie-Claire Mallison and Samantha Cruz are worthy of recognition for their excellent organization and program coordination.

References:

[1] Brown, D.. "Pd Plating (electroplating) - Palladium per Mil-P-45209." Palladium Plating. Professional Plating, 2008. Web. 19 Aug. 2013.

Deposition of the Immobilization Layer 3-Aminopropyltriethoxysilane on Gallium Nitride for Extremophile-Based Biosensors

Tiffany Huang
Electrical and Computer Engineering, Baylor University

NNIN REU Site: Stanford Nanofabrication Facility, Stanford University, Stanford, CA
NNIN REU Principal Investigator: Prof. Debbie G. Senesky, Aeronautics and Astronautics, Stanford University
NNIN REU Mentor: Ateeq Suria, Mechanical Engineering, Stanford University
Contact: tiffany_huang@baylor.edu, dsenesky@stanford.edu, asuria@stanford.edu

Abstract:

Biosensors composed of biomolecules and electromechanical components have enabled new sensing modalities for chemical sensing, pathogen detection and disease therapy. Traditional biosensors are silicon-based, but silicon has a known limited radiation lifetime. Gallium nitride (GaN), however, is radiation-hard and shows potential for use in biosensors to detect radiation. To support the development of a biosensor based on GaN and the radiation-tolerant extremophile bacteria *Deinococcus radiodurans* (*D. radiodurans*), we studied the attachment of an interfacial organosilane immobilization layer to GaN. More specifically, we attached 3-aminopropyltriethoxysilane (APTES) to GaN using molecular layer deposition. We defined the shape of the layer using die-level photolithography and lift-off, and we used goniometry, ellipsometry, and fluorescence microscopy to characterize the attachment properties of this layer. Optimization of this attachment will allow for long-lasting radiation detectors for applications such as medical radiation therapy and deep space exploration.

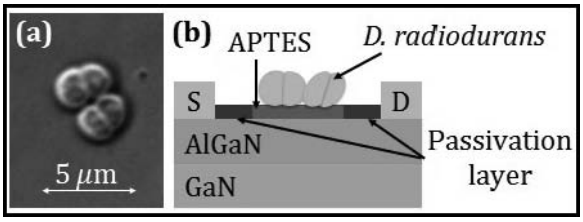

Figure 1: GaN biosensor HEMT device depiction.

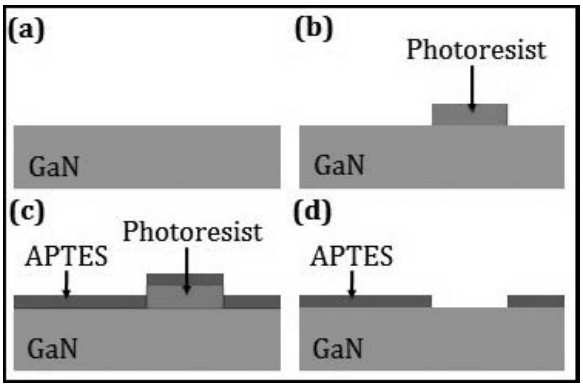

Figure 2: Process flow: (a) hydroxylation, (b) patterning of photoresist by photolithography, (c) deposition of APTES, and (d) patterning of APTES by liftoff.

Introduction:

Biosensors are biomedical or biological microelectromechanical systems (BioMEMS), systems that combine microelectronic materials such as semiconductors with biological components such as bacteria. These systems are largely used for biomedical or biological purposes such as diagnosing DNA and protein arrays [1]. By utilizing biological components composed of radiation-resistant extremophiles, biosensors may also be used in radiation-intense environments to detect radiation.

While traditional biosensors are silicon based and have a limited radiation lifetime [2, 3], gallium nitride (GaN) has a high radiation lifetime due to its large band-gap [4], making GaN ideal for radiation detection. The extremophile bacteria *Deinococcus radiodurans* (*D. radiodurans*) is also radiation-resistant [5, 6] and responds to radiation by generating ions [6]. We intend to combine *D. radiodurans* with GaN to build a biosensor that operates as a high-electron mobility transistor (HEMT), which has a high sensitivity to ions [4]. The biocompatibility of GaN has been shown [4], but no information exists on functionalizing GaN for D. radiodurans. We intend to interface GaN to *D. radiodurans* with the immobilization layer 3-aminopropyltriethoxysilane (APTES) commonly used to functionalize surfaces for bacteria attachment. Figure 1 depicts this APTES layer in the context of the HEMT device. Deposition and characterization of APTES will contribute to understanding the functionalization of GaN and may allow for construction of a HEMT radiation detector.

Fabrication Procedure:

We performed the following fabrication procedure on GaN samples and on silicon samples, using the silicon samples as references. Figure 2 depicts the fabrication procedure, which began with exposing the samples to 3:1 piranha solution (3:1 sulfuric acid: hydrogen peroxide) for two ten-minute sessions to clean the surface of organic molecules and activate hydroxyl groups on the surface. These hydroxyl groups add to the native oxide of the surface and ensure chemical functionalization of this surface for APTES [7].

Next, we used photolithography to pattern the surface to optimize for the gate size and shape of the HEMT device concept. This photolithography step consisted of depositing hexamethyldisilazane, depositing 1 μm of photoresist (Shipley 3612), exposing the samples to UV light, and developing in MF-26A. We then deposited APTES by molecular layer deposition to promote a conformal monolayer of APTES, and we performed liftoff in acetone. This left a surface patterned with APTES.

Characterization and Results:

To confirm deposition of this immobilization layer, the samples were characterized before and after the deposition step using goniometry and ellipsometry. Goniometry, a commonly used method for detecting changes in surface morphology, measures the wettability of the surface by surface water contact angle (SWCA) measurements. Table 1 shows a significant change in contact angle, indicating deposition of APTES. We used ellipsometry to further confirm the deposition of APTES. Ellipsometry calculates film thicknesses by measuring the change in light polarization and then fitting this experimental data to a model based on refractive index. APTES has a similar refractive index as oxide and therefore can be modeled as an oxide [8]. Table 1 shows a significant change in oxide thickness, indicating deposition of APTES.

	Pre-APTES	Post-APTES	Difference
Goniometry data			
Patterned GaN:	53°	43°	-10°
Patterned Si:	52°	29°	-23°
Bare GaN:	< 5°	27°	+27°
Bare Si:	< 5°	15°	+15°
Ellipsometry data			
Bare GaN:	7.1 Å	8.7 Å	1.6 Å
Bare Si:	17.1 Å	23.4 Å	6.3 Å

Table 1: Goniometry and ellipsometry characterization. Patterned samples underwent hydroxylation and photolithography before deposition. Bare samples only underwent hydroxylation before deposition and were used as reference samples.

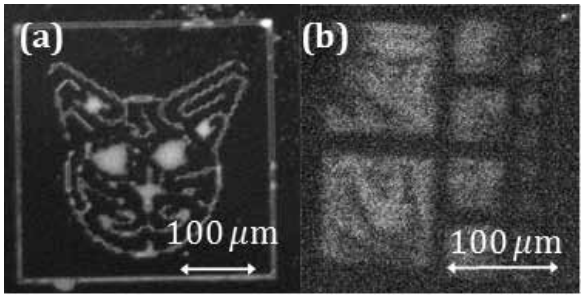

Figure 3: Fluorescence microscopy images of (a) cat and (b) square family on silicon. (See full-color version on inside cover.)

To verify patterning of the samples with APTES, the samples were characterized by fluorescence microscopy after liftoff. The samples were dyed with fluorescein isothiocyanate, which covalently binds with APTES and fluoresces at 510 nm (green light) when excited by 488 nm light (blue light). Figure 3 shows the fluorescently labeled samples, confirming patterning of the APTES.

Conclusions and Future Work:

Deposition and patterning of APTES on GaN were performed and characterized to support the development of a HEMT radiation detector. Future work includes investigating the attachment of *D. radiodurans* to APTES, and investigating the effectiveness of a *D. radiodurans* and GaN-based HEMT device for radiation detection.

Acknowledgments:

Many thanks to the following people and groups for their support: Ateeq Suria, Prof. Debbie G. Senesky, the XLab, Dr. Michael Deal, Maureen Baran, the NNIN SNF REU group, SNF staff and lab members, Cui Group, NNIN REU Program, and NSF.

References:

[1] R. Bashir, Adv. Drug Deliv. Rev., vol. 56, pp. 1565-1586, 2004.
[2] J. Howgate, Ph. D. dissertation, Dept. Physics, Walter Shottky Institut, Munich, Germany, 2012.
[3] G. Steinhoff, et al., Adv. Funct. Mater., vol. 13, pp. 841-846, 2003.
[4] M. Stutzmann, et al., Diamond Relat. Mater., vol. 11, pp. 886-891, 2002.
[5] G. GuanJun, et al., Chi. Sci. Bull., vol. 53, pp. 1675-1681, 2008.
[6] M. J. Daly, Nat. Rev. Microbiol., vol. 7, pp. 16-18, 2009.
[7] B. Baur, et al., Appl. Phys. Lett., vol. 87, pp. 263901, 2005.
[8] F. Zhang, et al., Amer. Chem. Soc., vol. 26, pp. 14648-14654, 2010.

PROC

Electrokinetic Characterization of Nanoscale Metal Oxide Films

Moath Othman
Materials Science and Engineering, San Jose State University

NNIN REU Site: Cornell NanoScale Science and Technology Facility, Cornell University, Ithaca, NY
NNIN REU Principal Investigator: Brian J. Kirby, Sibley School of Mechanical and Aerospace Engineering, Cornell University
NNIN REU Mentor: Alexander C. Barbati, Sibley School of Mechanical and Aerospace Engineering, Cornell University
Contact: moath.othman@gmail.com, bk88@cornell.edu, acb238@cornell.edu

Abstract:

In this work, we constructed a device to characterize the zeta potential of metal oxide films using electrokinetic forcing. In preparation, we characterized aluminum oxide tracer particles in a Malvern Zetasizer over a range of pH and salt concentrations. Then, we prepared oxide films of controlled thickness and chemistry, which were used to define a parallel-plate electrokinetic cell. With the particles suspended in fluids of varying salt concentrations and pH, we applied a voltage to generate an electroosmotic flow in the channel. Through measurements of the particle motion with particle image velocimetry (PIV) we could determine the zeta potential of the solid surface.

Introduction:

In micro- and nano-scale systems, electrokinetics plays an important role in determining the physical and chemical attributes of a system. Many solid surfaces become charged in the presence of a liquid due to (a) ionization of surface groups, and (b) adsorption of ions in solution onto a surface [1]. The charge of a surface will change as the salt concentration and pH of a solution are varied. The electrical potential, or zeta potential, is a measure of the electrokinetic properties of the surface.

Determination of the zeta potential of a surface in solutions of defined pH and salt concentration enables better understanding of the interactions between particles and surfaces. Knowledge of surface zeta potential is relevant to a wide variety of applications which involve a chemical interaction between particles and solutions.

$$u = \frac{-\varepsilon_0 \varepsilon}{\eta}(\zeta_p + \zeta_w)\nabla\phi$$

u: particle velocity
ζ_p: particle zeta potential
ζ_w: wall zeta potential
ϕ: external electric field
η: viscosity of solution
ε: electrical permittivity of solution

Figure 1: By measuring the velocity of particles under an electric field, we could characterize the zeta potential of the surface if the zeta potential of the particles was known.

In this work, we combined electroosmotic forcing and particle electrophoresis to determine the zeta potential of metal oxide surfaces in a custom built electrokinetic device. Using PIV, we could determine the velocity of a particle undergoing electrophoresis in an electroosmotic flow. The particle velocity can be used to determine the zeta potential of the wall, if the particle zeta potential is known, as shown in the equation in Figure 1 [2].

Particle Preparation and Characterization:

We first prepared solutions over a range of salt concentrations and pH; using sodium chloride (NaCl), we prepared 0.1 mM, 1 mM, and 10 mM solutions between pH 1 and 5, using HCl. We then cleaned the 700 nanometer alumina particles by mixing 0.03 grams of alumina particles in a 50 mL solution of deionized water, sonicating the particles to ensure proper dissolution, and centrifuging the particles for 20 minutes at 2500xg. The alumina particles would sediment to the bottom of the flask, and we exchanged the fluid in the flask for another 50 mL of deionized water. The process was repeated a total of three times, after which the particles were removed and dried in an oven for two hours. The particles were then mixed with solutions of known pH and salt concentration, and sonicated.

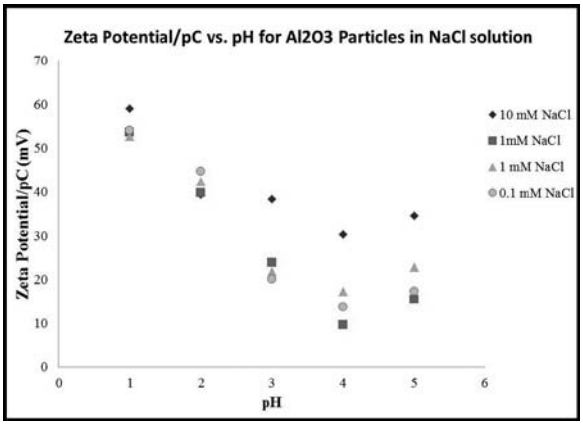

Figure 2: The zeta potential normalized by the counter ion concentration of the alumina particles showed a strong dependence on pH, but minimal variation with respect to salt concentration.

To characterize the zeta potential of the alumina particles, we used a Malvern Zetasizer Nano, which measures properties of suspended particles using dynamic light scattering. We characterized the particle zeta potential in the various solutions described above, as shown in Figure 2. Measured alumina particle zeta potentials were consistent with literature values [3].

Device Fabrication and Experimental Setup:

To fabricate the device, we deposited 300 nm of hafnium oxide (the material of interest) onto two 25 mm × 75 mm glass slides. One glass slide had two thru holes located 40 mm apart along the slide centerline. The two Hafnia substrates were assembled to sandwich a 127 μm Teflon® shim with a center removed, forming a 127 μm tall channel between the Hafnia surfaces. We sealed the edges with epoxy to prevent leaks. We fabricated large reservoirs above the thru holes to minimize surface tension effects and pressure gradients. A cross-section of the device is presented in Figure 3.

To run an experiment, we used a function generator, an amplifier, a voltmeter, two platinum electrodes, a camera, and a Nikon Eclipse TE2000-u inverted microscope. Initially, we filled the channel of our fabricated device with alumina particles suspended in solution. We then generated a square wave, amplifying the signal to our desired voltage, and used this field to actuate fluid in the device via platinum electrodes inserted in the reservoirs. The alumina particles suspended in salt solution could be tracked by taking a sequence of images using a camera, and the particle velocity could be measured via PIV. The experimental setup is shown in Figure 4.

Conclusions and Future Work:

In this work, we were able to successfully construct an electrokinetic device that can be used to determine the zeta potential of metal oxide films deposited on glass substrates. Our future work will be to calculate the zeta potential of hafnium oxide over a new range of pH using particle image velocimetry, fabricate similar devices for other metal oxide films, and improve the overall design of our device.

Acknowledgements:

I would like to particularly thank Dr. Brian Kirby and Alexander Barbati, as well as the Kirby research group and the Cornell NanoScale Facility staff at Cornell University. I'd also like to thank the National Nanotechnology Infrastructure Network Research Experience for Undergraduates (NNIN REU) Program and the National Science Foundation for making this experience possible.

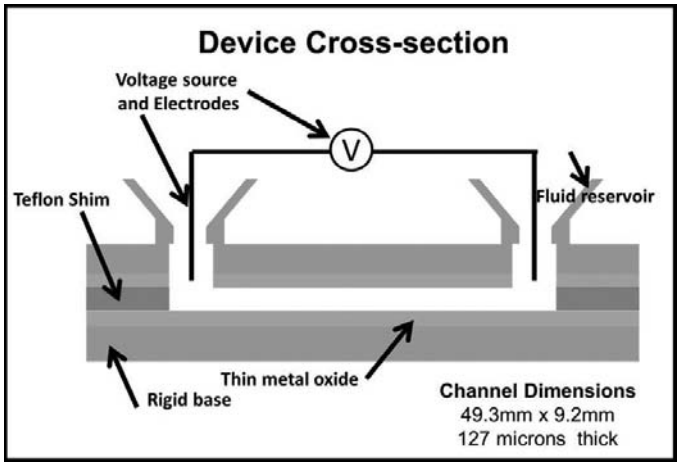

Figure 3: The relatively small channel thickness allowed us to assume 2D motion of alumina particles across the channel.

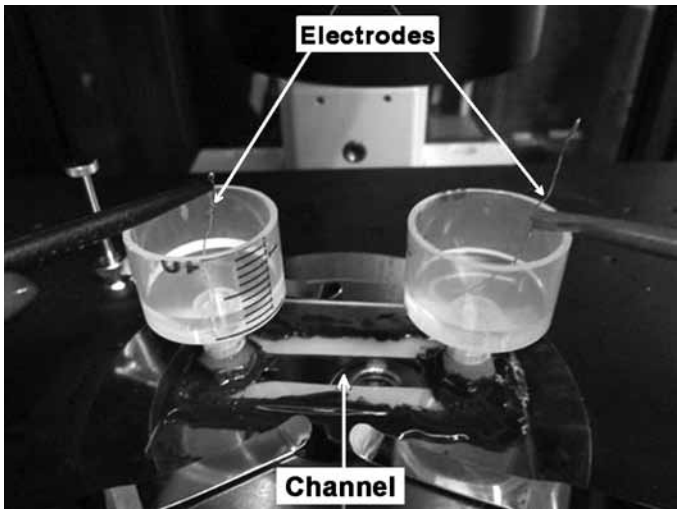

Figure 4: Using an inverted microscope and camera, we tracked alumina particles as they moved through the channel under an electric field.

References:

[1] Tandon, V., et al.; "Zeta potential and electroosmotic mobility in microfluidic devices fabricated from hydrophobic polymers: 1. the origins of charge"; Electrophoresis 29(5):1092-1101, 2008.

[2] Kirby, B.J.; "Micro- and Nanoscale Fluid Mechanics: Transport in Microfluidic Devices," Cambridge University Press, 2010.

[3] Bimal, P., et al.; J. of Colloid and Interface Science, pgs. 181-186 (2011).

Influence of Al_2O_3 Coating on the Annealing Behavior of Si Nanowires

Jaelin Quinn
Chemistry, Elizabeth City State University

NNIN REU Site: Nanotechnology Research Center, Georgia Institute of Technology, Atlanta, GA
NNIN REU Principal Investigator: Dr. Michael Filler, Chemical and Bimolecular Engineering, Georgia Institute of Technology
NNIN REU Mentors: Ildar Musin, Ho-Yee Hui, and Dr. Li-Wei Cho, Chemical and Biomolecular Engineering, Georgia Tech
Contact: quinn704@yahoo.com, michael.filler@chbe.gatech.edu, ildarm@gatech.edu, hhui3@gatech.edu, li-wei.chou@chbe.gatech.edu

Abstract:

Doped semiconductor nanowires have been utilized in many prototype energy harvesting, molecular detection, and plasmonic devices. The use of these materials, which are synthesized via the vapor-liquid-solid (VLS) technique, is dependent on the robust control of carrier concentration. To enable the electrical activation of previously incorporated dopant atoms, rapid thermal annealing (RTP) is generally required. However, due to rapid surface diffusion, silicon nanowires deform at temperatures (~1000°C) far lower than that expected from their bulk melting point (1414°C). To this end, we investigated conformal aluminum oxide (Al_2O_3) coatings as a route to suppress silicon (Si) atom surface diffusion and preserve nanowire structure. Al_2O_3 has a melting point around 2072°C. We studied how nanowire morphology was impacted under annealing in a nitrogen ambient for no more than one second at 900°C, 1000°C, and 1100°C, and used scanning electron microscopy (SEM) to analyze our data. We observed that none of the coated and non-coated nanowires melted, even at the highest temperature, which contradicts previous data collected under vacuum conditions in our laboratory. We then annealed the nanowires at the highest temperature (1100°C) for ten seconds and observed that the non-coated nanowires melted. We suspect the observed differences are due to the ambient chemistry and plan to test different gases, including Ar and H_2, in the future. Shorter annealing times will also be explored in attempt to fully map the process window.

Introduction:

The main goal of this research project was to suppress the Si atom surface diffusion with an Al_2O_3 coating. Al_2O_3 coats conformally, is very cost efficient, and forms a strong bond with Si nanowires, which makes it an ideal system to use in this experiment. Si is ubiquitous, which causes it to have an extensive knowledge base and many well-established methodologies. Dopants make Si conducive, however not all dopants may be active by taking up interstitial sites instead of substitutional in the diamond cubic crystal lattice. Thermal energy can activate dopants by allowing a dopant to take place of a silicon atom and become substitutional. In this experiment, phosphorus was our dopant, and in order for our dopant to be activated, annealing was necessary. Doped Si nanowires could be used for many applications such as plasmonic devices, which are devices that convert light into energy, energy harvesting such as solar cells, and molecular detection.

Experimental Procedure:

Researchers in this study performed atomic layer deposition (ALD), rapid thermal processing (RTP), and a scanning electron microscope (SEM) was used. Nanowires were grown using the vapor-liquid-sold technique. After the wires were complete, the gold was removed using an aqua regia solution. Researchers used two samples, one with Al_2O_3 coating and one without. Using ALD, we first coated the gold-removed Si nanowires with 30 nm of Al_2O_3 at 250°C. We then used RTP to spike-like anneal both samples of our nanowires at ~ 900°C, ~ 1000°C, and ~ 1100°C for less than one second. We also annealed our wires at the highest temperature (~1100°C) for ten seconds. During the annealing process, we used a continuous flow of nitrogen throughout the chamber. SEM was used to analyze our data.

Results and Conclusions:

In conclusion, we observed that the coated and non-coated nanowires that were annealed for less than one second did not melt. We believe that the non-coated nanowires remained in tact longer than expected may have occurred due to the continuous flow of the ambient gas, nitrogen, during the annealing process, which cooled down the nanowires. We also observed that when we annealed the nanowires for ten seconds at 1100°C, the alumina coating protected the wires from melting, and the non-coated wires were completely melted.

Future Work:

In the future, shorter annealing times could be applied to see if that affects the morphology of the nanowires. Also, we could test to see if different ambient gasses such as argon or hydrogen would have a major effect on the preservation of nanowires while being annealed.

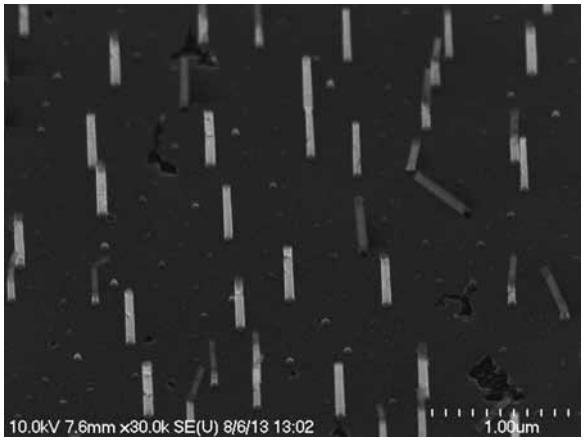

Figure 1: Nanowires coated with Al_2O_3, annealed at the highest temperature (1100°C) for one second.

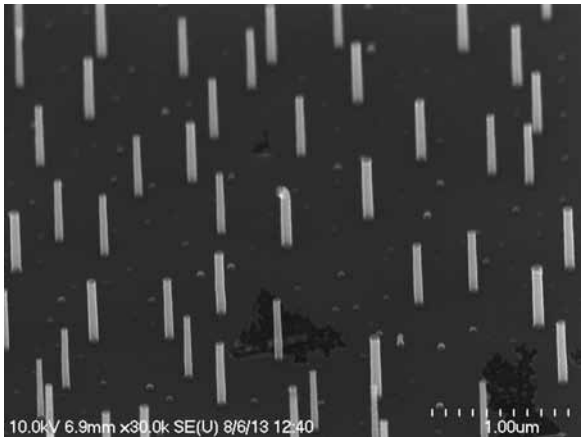

Figure 2: Nanowires with no coating, annealed at the highest temperature (1100°C) for one second.

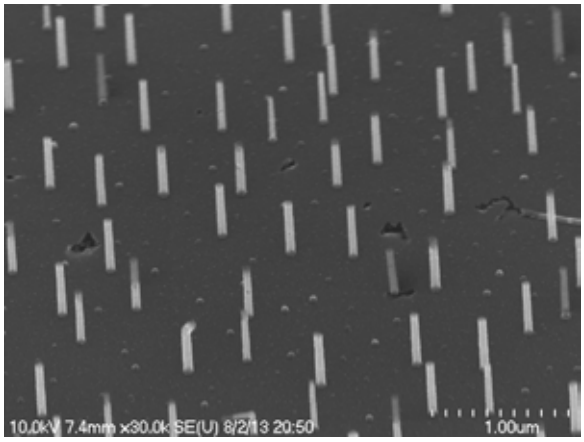

Figure 3: Nanowires coated with Al_2O_3, annealed at the highest temperature (1100°C) for ten seconds.

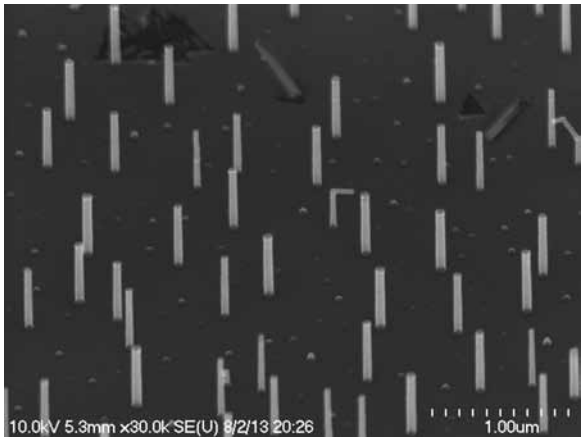

Figure 4: Nanowires with no coating, annealed at the highest temperature (1100°C) for ten seconds.

Acknowledgements:

I would like to thank Dr. Michael Filler, Ildar Musin, Ho-Yee Hui, Dr. Li-Wei Chou, and the entire Filler research group for there support and guidance throughout my internship. I would also like to thank Mrs. Leslie O'Neil, Dr. Nancy Healy, and Ms. Melanie-Claire Mallison for being such great program coordinators and showing strong commitment to the NNIN REU Program at Georgia Tech. Furthermore, I would like to thank the cleanroom staff at Georgia Tech for their great training, especially John Pham for taking time out to assist me during procedures when needed. Also, I would like to thank the E-Spare Program of Elizabeth City State University and Quachel Bazile (2012 NNIN REU), ECSU Alumni for helping me throughout my journey. Finally, I would like to thank the National Nanotechnology Infrastructure Network Research Experience for Undergraduate Program and the National Science Foundation for their support and funding.

References:

[1] Chou, Li-Wei, Dr., and Michael A. Filler, Prof. "Engineering Multimodal Localized Surface Plasmon Resonances in Silicon Nanowires." Wiley College. Onlinelibrary.wiley.com. DOI: 10.1002/anie.201301468, 13 June 2013.

[2] Chou, L.-W., Dr., N. Shin, S.V. Sivaram, and Prof. M.A. Filler, "Tunable Mid-Infrared Localized Surface Plasmon Resonances in Silicon Nanowires." J. Am. Chem. Soc., 134 (39), pp 16155-16158, DOI: 10.1021/ja3075902, September 2012.

[3] Min, B., J.S. Lee, K. Cho, J.W. Hwang, H. Kim, M.Y. Sung, S. Kim, J. Park, H.W. Seo, S.Y. Bae, M.-S. Lee, S.O. Park, and J.-T. Moon. "Semiconductor Nanowires Surrounded by Cylindrical Al_2O_3 Shells. Journal of Electronic Materials, 32.11, 1344-348 (2003).

Deposition and Characterization of Magnetic Permalloy for Future Endomicroscope Actuators

Joseph Rivas
Mechanical Engineering, Binghamton University

NNIN REU Site: Lurie Nanofabrication Facility, University of Michigan, Ann Arbor, MI
NNIN REU Principal Investigator: Kenn Oldham, Mechanical Engineering, University of Michigan
NNIN REU Mentor: Pilar Herrera-Fierro, Solid-State Electronics, and Electrical Engineering, University of Michigan
Contact: jrivas2@binghamton.edu, oldham@umich.edu, pilarhf@umich.edu

Introduction:

When nickel and iron are combined in an 80% to 20% ratio, respectively, the resulting material is called permalloy. Permalloy expresses strong magnetic properties and as such, is a prime candidate for future actuator applications. The biomedical community has taken recent interest in the development of permalloy structures. One potential application in that field is as an alternative to comparatively large piezoelectric actuators currently used in novel prototype endomicroscopes. The use of permalloy will be attempted in order to produce smaller actuators that will instead apply a magnetic field to control lens movement. This project aimed to characterize the different permalloy films that were plated when variables such as current density, plating duration, and pulse timing were varied in the electroplating process.

Oxide-coated wafers were deposited with a chrome-gold seed layer and a secondary oxide coating on the back provided insulation. Photoresist was developed on wafers after electroplating, and was removed in order to begin etching. Ferric chloride, gold etch, and CR-14 etchants were used to etch to the oxide; plasma etch machines etched the oxide and the silicon in order to create cantilevers. A magnetic field was finally applied to test the magnetic properties of these permalloy cantilevers.

Experimental Procedures:

A typical electroplating process requires that a wafer be coated with a conductive seed layer and patterned with photoresist prior to the plating. A seed layer consisting of 500Å of gold and 300Å of chrome was deposited onto the oxide wafers with an EnerJet Evaporator tool. Subsequently, KMPR photoresist was spun at 3000 rpm in order to produce a film 9-10 μm thick. Various different masks were initially used in order to characterize the plating rate and experiment with the current density. Wafers were inserted into a nickel-iron electroplating solution. A dummy was plated for ten minutes at a current density of 20 mA/cm^2 in order to prepare the ion flow in the solution. Wafers were then plated at several different current densities for varying amounts of time. The plating program for the electroplating process consisted of a forward current pulse 90 ms on and 10 ms off for a total pulse duration of 100 ms. After a primary energy dispersive x-ray spectroscopy (EDX) analysis with a scanning electron microscope, it was concluded that a lower current density provided a higher concentration of nickel. Once the permalloy was plated, the photoresist was stripped with acetone and Remover PG.

The permalloy structures were inspected with the Olympus BX-51 microscope and the LEXT Interferometer in order to measure surface roughness and determine if there was any remaining photoresist. A wet etch procedure was conducted with gold etch and CR-14 chrome etch in order to strip the seed layer; a 40 second gold etch produced a substantial undercut in the permalloy features, causing them to fall off.

A different approach was attempted in order to reduce the undercut and produce useful permalloy structures. Thus, permalloy was then plated directly onto the seed layer. Furthermore, the seed layer thickness was reduced to 75Å of chrome and 250Å of gold. Since the permalloy was being plated onto a bare surface, the resulting films were extremely stressed and were peeling at the edges of the wafer.

The plating program was gradually modified to include a reverse current and adjusted pulse timing, as seen in Figure 1. The reverse current allowed the ions to ease off the wafer before being plated, thus reducing the film stress and providing a smoother film.

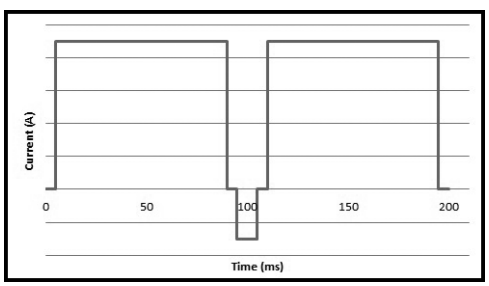

Figure 1: Final pulse timing.

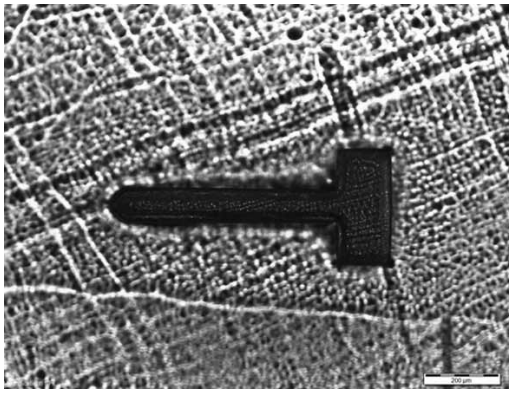

Figure 2: Completed cantilever.

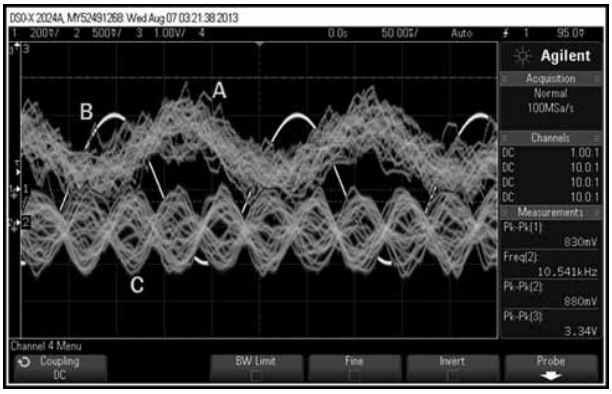

Figure 3: Oscilloscope readings.

The permalloy wafers were then spun with AZ-9260 photoresist. Exposure times for a permalloy base are not given, so we used the same exposure time as one would use for a gold base, in this case 90 seconds (s). The wet etch was attempted again, though this time the excess permalloy was etched with ferric chloride, an etchant typically used for copper. The permalloy structures still suffered from severe undercut, compromising the structural integrity of the cantilevers and rendering them unusable. The etching was characterized and it was determined that 43 seconds of ferric chloride, 18 s of gold etch and 7 s of CR-14 produced stable permalloy features.

Once the seed layer was stripped, the wafers went through a 30 minute plasma etch on the Plasmatherm 790 tool in order to remove the 8000Å oxide layer. The wafers were then subjected to an anisotropic xenon difluoride (XeF_2) etch in order to undercut the cantilever structures and release them from the wafer base. This process ran for a total of 230 cycles at 30 seconds each. Figure 2 shows a cantilever after all the etching has been completed.

Results and Future Work:

After the cantilevers were created, they were tested by applying a magnetic field generated from running a current through a coil. A Laser Doppler vibrometer was placed over the cantilevers in order to measure the vibration of the cantilevers. Frequency sweeps were conducted in an attempt to find the resonant frequency, but most of the input frequencies produced no noticeable patterns from the cantilevers. As seen in Figure 3, wave C shows that a certain frequency did produce some kind of pattern on the cantilevers. Though the LDV did measure a pattern, this was enough to prove the strength of the permalloy films. It is also possible that the LDV was picking up a different motion. More accurate testing must be done in order to confirm that permalloy is indeed a viable alternative to the lead zirconate titanate (PZT) material that is currently used in endomicroscope actuators.

Acknowledgements:

This work would not have been possible without the generosity and guidance of my PI Kenn Oldham and mentor Pilar Herrera-Fierro. I would also like to thank the entire Wet Chemistry Laboratory team for their help and insight. I am indebted to the National Science Foundation and the NNIN REU Program for this opportunity.

PROC

Infrared Photodetectors with Two Dimensional Materials

Andrew Stephan
Physics Department, Bethel University

NNIN REU Site: Minnesota Nano Center, University of Minnesota-Twin Cities, Minneapolis, MN
NNIN REU Principal Investigator: Dr. Steven J. Koester, Electrical and Computer Engineering Department, University of Minnesota
NNIN REU Mentor: Yoska Anugrah, Electrical and Computer Engineering Department, University of Minnesota
Contact: aws33656@bethel.edu, anugr002@umn.edu, skoester@umn.edu

Abstract:

In this work, a new heterostructure photodetector has been designed using monolayer graphene and varying thicknesses of molybdenum disulfide. This device could provide sensitivity in the infrared (IR) region optimal for optical communication, 1550 nanometers (nm), while maintaining low dark current. Monolayer graphene grown by chemical vapor deposition (CVD) has been patterned onto mechanically exfoliated molybdenum disulfide (MoS_2) and titanium-gold (Ti-Au) contacts made to both materials. Initial electrical characterization of the devices has been performed. The resulting resistance and linearity of the contacts agree with predictions. Infrared probing of the device at 1550 nm indicates either more surface area or a different wavelength is required.

Introduction:

As computer processor speed rises exponentially, the bandwidth required for inter-processor communication grows as well. Integrated optoelectronics may solve the interconnect bandwidth bottleneck. The three necessary components are infrared transmitters, modulators and detectors. The field of infrared transmission is already a mature science, and some progress has been achieved with experimental infrared modulators with signs of future success. The remaining piece of the puzzle is suitable infrared photodetectors. The unique properties of two dimensional (2D) materials could be the key to their construction, helping to realize the next generation of high-speed optical communications.

Device Concept:

Previous attempts to construct an IR photodetector with 2D materials focused on graphene, which absorbs radiation over a wide wavelength range spanning from the far infrared to the visible. However, graphene is problematic because of its high conductivity. Any voltage applied to collect charge carriers freed by radiation will also cause non-photoinduced current, or dark current. This dark current is on the same order as the photocurrent from an ordinary source, resulting in a low signal-to-noise ratio. To circumvent this issue, MoS_2 was incorporated

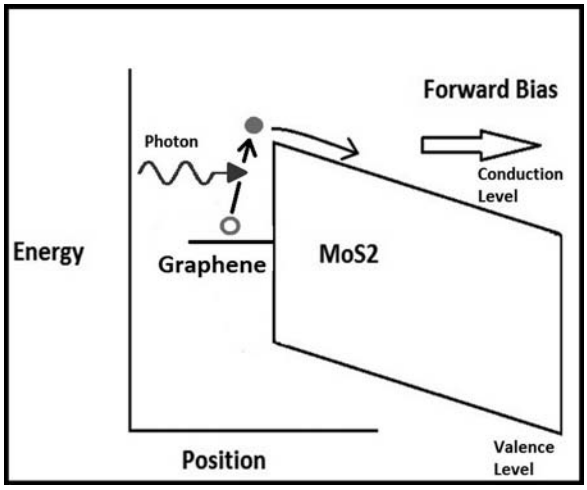

Figure 1: Envisioned operation in the new device. An infrared photon induces a graphene carrier to make the leap into the MoS_2's conduction band, where it is carried away by the applied bias, thus producing a signal. The photon must carry at least enough energy to overcome the graphene-MoS_2 barrier.

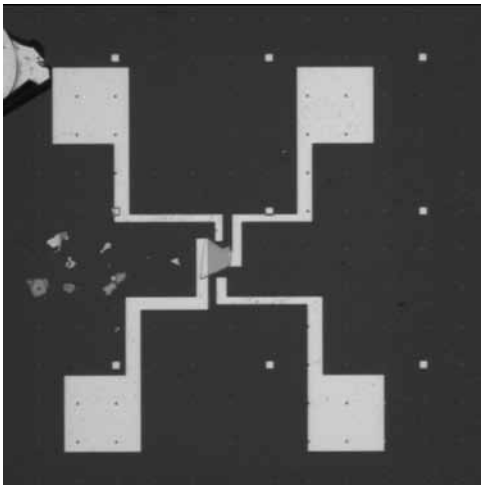

Figure 2: A completed device. The central piece is a flake of MoS_2 of approximately 50 µm by 50 µm. Atop this is a nearly-transparent piece of graphene. A pair of Ti-Au contacts overlaps the edge of each material.

into the device to introduce a band-gap, which minimizes dark current, thus improving the signal. It is believed that the Fermi level in graphene is between the conduction and valence bands of bulk MoS_2. Since the gap exceeds the energy contained in a 1550 nm photon, it should be possible to gate the device so as to induce an energy barrier between the graphene and MoS_2 which corresponds to 1550 nm. This is both the device's absorption and noise-reduction mechanism.

Fabrication Sequence:

A sequence of fabrication steps was developed to produce these devices. The first step was using electron-beam lithography (EBL) and electron beam evaporation (EBE) to attach an alignment grid onto the chosen substrate — in this case, a silicon dioxide and silicon wafer. The second step was mechanical exfoliation of MoS_2 onto the wafer and location of suitable flakes. After their locations were mapped out, a large sheet of monolayer graphene was removed from its copper foil and placed over the substrate. Then EBL was used to pattern a resist polymer onto the flakes to protect certain areas of the graphene sheet. A light oxygen plasma removed the uncoated areas of graphene. Finally EBL and EBE were applied once more to lay down metallic contact pads on the graphene and MoS_2.

Characterization:

After some devices were completed, they were tested by measuring the current induced by applying voltages between the graphene-graphene, graphene-MoS_2, and MoS_2-MoS_2 contact combinations. The resulting I/V characteristics showed that the electrical contacts were alive and behaved as expected. The graphene-graphene characteristic was linear, indicating an Ohmic contact with a resistance of approximately 27 kΩ. The MoS_2-MoS_2 and graphene-MoS_2 tests, on the other hand, exhibited behavior reminiscent of a Schottky barrier, producing asymmetric I/V characteristics whose linear approximations give resistances of approximately 67 MΩ and 33 MΩ. These preliminary results suggest photodetector should be detectable with this device.

However when the same characterizations were performed with an IR laser incident on the sample, no significant change was recorded. There are several possible explanations for this. First, the testing stage used required that the fiber carrying the IR signal be several millimeters over the sample, causing the beam to diverge drastically. Another possibility is that the junction region will not absorb 1550 nm light. This could be rectified by gating the junctions appropriately to shift the Schottky barrier. Another possibility is that the device's small surface area did not allow enough absorption for an appreciable photocurrent, but this seems less likely as other detectors of a similar size have been fashioned from graphene alone.

Future Work:

There is a vast amount of progress left to be made. The very first step, as mentioned above, is to achieve photodetection in the ideal region near 1550 nm. Subsequently various optimizations must be performed to determine the ideal size, thickness and possibly shape of the MoS_2 flakes that should be used. Monolayer, or 2D, MoS_2 should be an area of special interest due to its unique band structure. If these devices can be made as effective as is hoped, then a more efficient exfoliation process must also be found so as to make mass production a more realistic goal.

Conclusions:

A new heterostructure photodetector using 2D materials has been proposed, a fabrication sequence developed and prototypes constructed. Initial characterizations show promise but much work remains before actual photodetection is measured. If the potential of these devices is realized they could replace current electronic communications systems, greatly enhancing computational data transfer bandwidth.

Acknowledgements:

I would like to thank Dr. Steven Koester and my mentor Yoska Anugrah for helping me at every step of the way, and the National Science Foundation, the National Nanotechnology Infrastructure Network Research Experience for Undergraduates (NNIN REU) Program, and the University of Minnesota for making this research possible.

Electron Transfer Dynamics in Polymer Solar Cells Studied by Femtosecond Transient Absorption Measurements

Andrew Tam
Electrical Engineering, Rice University

NNIN iREU Site: National Institute for Materials Science (NIMS), Tsukuba, Ibaraki, Japan
NNIN iREU Principal Investigator: Dr. Kohei Uosaki, Director General of Global Research Center for Environment and Energy based on Nanomaterials Science (GREEN), National Institute for Materials Science (NIMS)
NNIN iREU Mentors: Dr. Hidenori Noguchi, Nano Interface Group, National Institute for Materials Science (NIMS); Dr. Mikio Ito, Global Research Center for Environment and Energy based on Nanomaterials Science (GREEN), National Institute for Materials Science (NIMS)
Contact: andrew.m.tam11@gmail.com, uosaki.kohei@nims.go.jp, noguchi.hidenori@nims.go.jp, ito.mikio@nims.go.jp

Abstract and Introduction:

Organic molecules offer a cheaper alternative to traditional bulk crystalline materials for solar cells. Unfortunately, none have yet shown efficiencies as high as those in silicon devices. Efficient solar cell materials must have an electronic band gap suitable for absorbing most of the radiation emitted by the sun, optimally 1.1-1.4 eV. So far, the band gaps of all organic polymers created for this purpose have been much higher or the molecules have been insoluble, preventing cheap production of efficient polymer solar cells. To improve the cost-efficiency of polymer solar cells, new soluble molecules are needed with smaller band gaps. PDTNT-DPPOD is a new such organic molecule synthesized by Dr. Yasuhiro Shirai of the Japanese National Institute for Materials Science (NIMS). It has a band gap of 1.37 eV and can act as an electron donor when paired with PCBM or C60 acceptor molecules.

In actual devices, however, the short-circuit current and open circuit voltages were lower than expected. In order to understand why, we use pump-probe spectroscopy to determine if electrons are being excited in the donor molecule and transferred to the acceptor molecules in solution.

Experimental Procedure:

We made three solutions of PDTNT-DPPOD dissolved in ortho-dichlorobenzene: PDTNT-DPPOD, PDTNT-DPPOD with PCBM, and PDTNT-DPPOD with C60. In all solutions, the concentration was 1 mg/mL. The mass ratio between PDTNT-DPPOD and PCBM/C60 was 1:1. For each pump-probe measurement, a 0.2 mm thick layer of one solution was flowed through a flow-cell using a 35 hz vibration pump. A pump pulse of 700 nm and a probe pulse of 670 nm were shone on the sample and the absorbance of the probe pulse was recorded. The delay between the two pulses was varied over a range of about 60 picoseconds. For the solutions of PDTNT-DPPOD alone and PDTNT-DPPOD with PCBM, the pump power was 10 mW and the probe power was 6 mW, at a repetition rate of 1 kHz. For the solution of PDTNT-DPPOD and C60, the pump power was 10 mW and the probe power was 4 mW at 1 kHz repetition, but the repetition was then lowered to 100 Hz to allow the system to return to the ground state between data point collection.

Results and Conclusions:

Pump-probe measurements of all three solutions showed a clear decrease in absorbance at zero delay between the pump and probe pulses. This indicates promotion of the ground state electrons to higher energy states, resulting in an absence of electrons that would have otherwise absorbed the probe pulse. We define the peak to steady-state ratio as the maximum decrease in absorbance over the end behavior decrease in absorbance (A/B in the figures).

PDTNT-DPPOD alone had the largest peak to steady-state ratio of 7.3, indicating most electrons excited by the pump pulse returned to the ground state 50 picoseconds later (Figure 1). The decay of the absorbance decrease was fitted by a two-exponential function with a fast portion corresponding to the singlet state decay and a slower portion corresponding to triplet state decay. PDTNT-DPPOD with PCBM had a lower peak to steady-state ratio of 4.9 indicating some electrons were captured by the PCBM acceptor and prevented from returning to the ground state (Figure 2). The decay still showed two separate exponential components corresponding to the singlet and triplet state decays however, indicating that many excited electrons were not captured. PDTNT-DPPOD with C60 had the lowest peak to steady-state ratio of 2.6, indicating a more efficient electron transfer than with PCBM (Figure 3). Additionally, the decay function had only a slow exponential component; the lack of an observed fast decay rate back to the ground state indicates efficient singlet charge transfer to the C60.

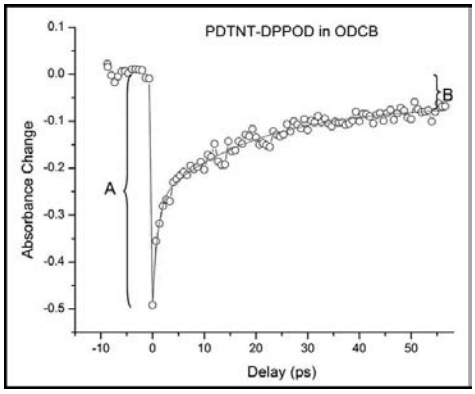

Figure 1: PDTNT-DPPOD undergoes rapid electron excitation, followed by a two-part exponential decay.

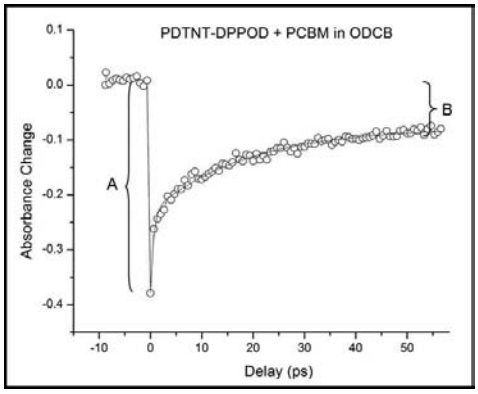

Figure 2: PDTNT-DPPOD with PCBM's moderate decrease in absorption indicates weak electron transfer.

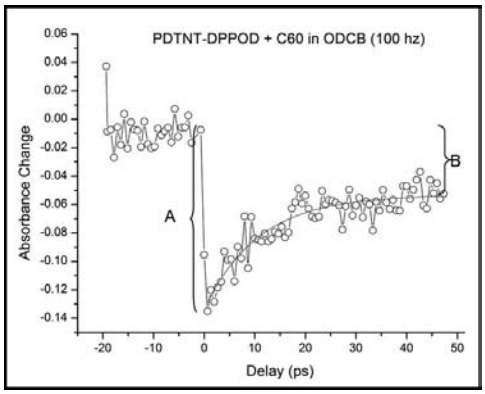

Figure 3: PDTNT-DPPOD with C60 has almost twice the absorption decrease of PCBM, indicating more efficient electron transfer.

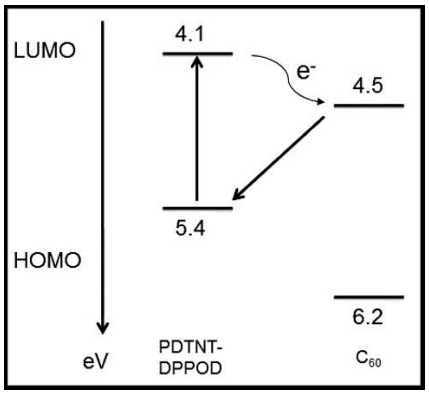

Figure 4: Electron excitation, charge transfer, and return to ground state/HOMO in PDTNT-DPPOD and C60.

PDTNT-DPPOD with C60 was originally measured at a repetition rate of 1 kHz, but that measurement never reached steady state. The measurement had to be repeated at 100 Hz because the absorbance of the system took longer to recover than for PDTNT-DPPOD alone. This indicates that charge transfer occurred from PDTNT-DPPOD's lowest unoccupied molecular orbital (LUMO) to C60's LUMO, which then had a longer recovery time back to PDTNT-DPPOD's highest occupied molecular orbital (HOMO) than from PDTNT-DPPOD's LUMO (Figure 4). This confirms device testing results that C60 served as a better electron acceptor than PCBM.

Future Work:

We have determined that the electron transfer process between PDTNT-DPPOD and PCBM is inefficient, likely because there is only a 0.1 eV difference in their LUMO energy levels. However, it is still unclear why solar cells made with PDTNT-DPPOD and C60 exhibit such low short-circuit current and open circuit voltage when compared with other molecules synthesized by Dr. Shirai's group. Fluorescence studies are needed to characterize the absorption wavelengths of different charge species for this molecule. To better understand device performance, nanosecond pump-probe measurements can be performed to determine carrier lifetime and recombination timescales. Solutions and films of thiophenes have also been known to exhibit different characteristics, so experiments should be performed with the film phase of this molecule.

Acknowledgments:

I would like to thank Dr. Kohei Uosaki, Dr. Hidenori Noguchi, Dr. Mikio Ito, Dr. Yasuhiro Shirai, NIMS, NSF, and the NNIN iREU Program for all their help and generosity.

References:

[1] Cook, S., Furube, A., and Katoh, R. Analysis of the excited states of regioregular polythiophene P3HT. Energy and Environmental Science, 1(2), 294-299. (2008).

[2] Guo, J. J., Ohkita, H. H., Benten, H. H., and Ito, S. S. Near-IR femtosecond transient absorption spectroscopy of ultrafast polaron and triplet exciton formation in polythiophene films with different regioregularities. Journal of the American Chemical Society, 131(46), 16869-16880. doi:10.1021/ja906621a (2009).

PROC